Experimental investigations of charging/melting cycles of paraffin in a novel shell and tube with longitudinal fins based heat storage design solution for domestic and industrial applications

Zakir Khan [a]*, Zulfiqar Ahmad Khan [a]

[a] Bournemouth University, Faculty of Science and Technology, NanoCorr, Energy and Modelling (NCEM), Fern Barrow, Talbot Campus, Poole, Dorset BH12 5BB, UK.

E-mail: zkhan@bournemouth.ac.uk

Corresponding Author:

[a]* Bournemouth University, Faculty of Science and Technology, NanoCorr, Energy and Modelling (NCEM), Fern Barrow, Talbot Campus, Poole, Dorset BH12 5BB, UK.

E-mail: zkhan2@bournemouth.ac.uk

Tel.: +44 7459249069

Abstract

Due to vulnerability of solar energy based technologies to weather fluctuations and variations in solar thermal irradiance, thermal energy storage (TES) systems with their high thermal storage capacity offer a sustainable solution. In this article, experimental investigations are conducted to identify thermal performance of latent heat storage (LHS) unit in connection with flat plate solar collector during charging cycles. LHS unit is comprised of novel geometrical configuration based shell-and-tube heat exchanger with longitudinal fins, paraffin as thermal storage material and water as heat transfer fluid (HTF). In order to overcome the effect of low thermal conductivity of paraffin, the effective surface area and overall thermal conductivity for heat transfer is significantly improved by employing longitudinal fins. Moreover, the vertical orientation of longitudinal fins supports natural convection, which can assure rapid charging of paraffin in LHS unit. In experimental tests, the focus is on probing the heat transfer mechanism and temperature distribution in entire novel LHS unit, the influence of inlet temperature and volume flow rate of HTF on phase transition rate and mean power. Experimental results revealed that natural convection significantly influences the phase transition rate. Therefore, enthalpy gradient is noticed between paraffin at top, central and bottom positions in LHS unit. Likewise, the phase transition rate and mean power of LHS unit is significantly increased by a fraction of 50.08% and 69.71% as the inlet temperature of HTF is increased from 52 ^{o}C to 67 ^{o}C, respectively. Similarly, it is concluded that volume flow rate of HTF has a relatively moderate influence on thermal performance; however the influence declines with an increase in inlet temperature of HTF. Due to significant enhancement in thermal performance, the novel geometrically configured LHS unit can accumulate about 14.36 MJ of thermal energy in as less as 3 hours. Furthermore, a broad range of domestic and commercial energy demands can be fulfilled by simply assembling several LHS units in parallel sequence.

Keywords

Thermal energy storage, Latent heat storage, Phase change material, Shell-and-tube heat exchanger, Heat transfer, Natural convection.

1. Introduction

Energy is the backbone of a country economic development. Due to rapid increase in industrial and domestic energy demands, the dependency on fossil fuels to meet required energy demands have further increased. However, the excessive usage of fossil fuels have provoked global warming and climate change [1, 2]. Therefore, in order to limit environmental pollutions and to meet energy demands, developments in technologies are essential to utilise renewable energy sources. Solar energy is considered as a crucial renewable energy source due to its clean, free of cost and worldwide distribution of incident solar radiations [3, 4]. However, the fragmentary and inconsistent nature of solar radiations has affected the widespread applications of solar energy. To overcome the inconsistent and unpredictable nature of solar energy, TES system can provide a feasible solution. TES system can be utilised to capture thermal energy at solar peak hours and release it at solar off peak hours or night times. To shorten the energy supply and demand gap, LHS systems can be employed due to their higher thermal storage density, phase change materials (PCM) availability at wide range of temperatures, higher latent heat capacity at almost isothermal condition and lower vapour pressure [5, 6].

LHS systems are employed in number of applications including solar thermal systems, energy management and peak-shaving, waste heat recovery, building heating and air conditioning, agricultural drying units and automobile [7-13]. However, the widespread practical utilisation of LHS system is still under the influence of low thermal conductivity (≈ 0.2 – 0.4 W/m.K) of PCM, which handicaps the rapid charging and discharging of thermal energy [14]. Therefore, to improve thermal performance of LHS system, efficient and responsive heat exchanging techniques are essential to be adopted. A substantial number of research articles have been published that concern developments in thermal performance of LHS system including geometrical configuration [15], using extended surfaces [16], addition of thermal conductive additives [17], form stable and encapsulation of PCM [18, 19].

Thermal performance of LHS system is highly influenced by geometrical configuration of heat exchanger. Therefore, this article is focused on shell-and-tube heat exchanger based LHS systems due to the fact that it presents relatively better heat transferring performance and possesses excellent integration to number of engineering applications [20]. Wang et al. [21] conducted numerical investigations to examine thermal performance of n-octadecane in horizontal shell-and-tube heat exchanger. It was observed that with an increase in inlet temperature of HTF, the phase transition time was significantly reduced and the amount of thermal energy stored was non-linearly increased. However, with an increase in mass flow rate, the melting time was reduced whereas the amount of thermal storage was not significantly affected. Similarly, Tay et al. [22] performed experimental investigations on thermal performance of water as PCM in vertical tubes-in-tank heat exchanger. It was observed that an increase in mass flow rate from 0.01 kg/s to 0.07 kg/s reduced the phase transition duration from 215 min to 88 min. Hosseini et al. [23] conducted an experimental and numerical study to identify the influence of natural convection and inlet temperature of HTF on phase transition rate of paraffin in horizontal shell-and-tube heat exchanger. It was reported that natural convection highly influenced melting rate of paraffin in upper portion of shell. Likewise, it was noticed that the melting time was reduced by a fraction of 37% with an increase in inlet temperature from 70 ^{o}C to 80 ^{o}C. Likewise, Meng and Zhang [24] conducted an experimental and numerical investigation of melting behaviour of paraffin composite with copper form in vertical shell-and-tube heat exchanger. It was noticed that due to natural convection the temperature at top portion was higher as compared to other portions. Likewise, with an increase in inlet temperature of HTF from 75 ^{o}C to 85 ^{o}C, the melting time was reduced by a fraction of 41.67%. Moreover, an increase in flow velocities

of HTF from 0.1 m/s to 0.2 m/s had only reduced the melting time by 15.1%. Furthermore, Esapour et al. [25] numerically investigated the melting behaviour of paraffin in horizontal shell-and-tube heat exchanger. It was noticed that with an increase in number of HTF tubes from 1 to 4, the melting time was reduced by 29%. Likewise, Luo et al. [26] numerically examined the effect of HTF tubes number and their orientations in horizontal shell-and-tube heat exchanger on thermal performance. It was noticed that melting time for single HTF tube was 5 times as compared to nine HTF tubes case. Likewise, centrosymmetric configuration showed better thermal performance than staggered and inline configurations.

It can be construed from previous literature that shell-and-tube heat exchanger configurations have significant influence on thermal performance of LHS system. However, the optimal advantages are still hindered by low thermal conductivity of PCM. Therefore, the most appropriate and cost effective technique to enhance thermal performance is to incorporate extended surfaces. Rathod and Banerjee [27] conducted an experimental examination of melting behaviour of stearic acid in vertical shell-and-tube heat exchanger with three longitudinal fins configuration. It was observed that with longitudinal fins, the melting time was reduced by 24.52% as compare to no fins orientation. Yuan et al. [28] examined the impact of longitudinal fins on melting rate of lauric acid in horizontal shell-and-tube heat exchanger. It was noticed that complete melting time was reduced from 328 min for no fins orientation to 180 min for two fins orientation. Likewise, the peak melting enhancement ratio for inlet temperatures of 60 ^{o}C, 70 ^{o}C and 80 ^{o}C were 1.403 to 1.362, and 1.328, respectively. Li and Wu [29] conducted numerical investigations on thermal performance of $NaNO_3$ in horizontal shell-and-tube heat exchanger with and without longitudinal fins. It was noticed that average total heat flux of heat exchanger was increased by inclusion of six longitudinal fins and consequently, the melting time was reduced by 20%. Rabienataj Darzi et al. [30] numerically examined the influence of number of fins on melting time of n-eicosane in horizontal shell-and-tube heat exchanger. It was reported that as compared to no fins orientation, the melting time was reduced by 39%, 73%, 78% and 82% by incorporating 4, 10, 15 and 20 fins, respectively. However, with an increase in number of fins, the influence of natural convection on melting rate was affected. Likewise, Tao and He [31] recommended that non-uniform melting front and temperature distribution caused by natural convection could be improved by inclusion of longitudinal fins. However, the uniformity could be distorted again if excessively large fins number, height and thickness are employed. Wang et al. [32] conducted numerical analyses to identify the impact of various angles between three longitudinal fins on thermal performance of PCM in horizontal shell-and-tube heat exchanger. The selected angles between adjacent fins were 30^{o}, 60^{o}, 90^{o} and 120^{o}. It was reported that fins angle 60^{o} and 90^{o} displayed better heat transfer enhancement. Moreover, Liu and Groulx [33] experimentally investigated the thermal behaviour of dodecanoic acid in horizontal shell-and-tube heat exchanger with four longitudinal fins configuration. Longitudinal fins were installed in two orientations such as straight and angled. It was reported that natural convection was a dominant mode of heat transfer. Likewise, it was observed that inlet temperature of HTF has more prominent impact on thermal behaviour as compared to flow rate of HTF. Also, it was reported that angled fins showed a slightly lower melting time as compared to straight fins. However, the impact of angled fins declined with an increase in inlet temperature.

Beside longitudinal fins, the other proposed design solutions for thermal performance enhancement with extended surfaces are radial, helical, pinned and triplex fins. Tay et al. [34] conducted numerical investigations on three models of tubes-in-tank heat exchanger configurations without fins, with pins and with radial fins. It was concluded that radial fins based heat exchanger had better phase transition rate and average effectiveness as compared to without fins and with pins orientations. However, a

comparative study illustrated that longitudinal fins possess better thermal storage performance. Caron-Soupart et al. [35] experimentally studied the melting behaviour, heat exchanger power and thermal storage density of three vertical shell-and-tube heat exchanger configurations. The three selected orientations were tube without fins, with longitudinal fins and with radial fins. It was observed that heat exchanger orientations with longitudinal fins and circular fins showed significantly higher melting rate as compared to no fins orientation. Likewise, heat exchanger power was augmented by a factor of 10 as compared to no fins orientation. However, thermal storage density was noticeably reduced by radial fins orientation as compared to no fins orientation. Similarly, Agyenim et al. [36] experimentally examined the thermal performance of erythritol in horizontal shell-and-tube heat exchanger with three varied orientations of no fins, circular fins and longitudinal fins. It was reported that longitudinal fins orientation showed comparatively better thermal performance. Hence, it can be deduced from literature that longitudinal fins in vertical orientation of shell-and-tube heat exchanger has better thermal performance in terms of phase transition rate, thermal storage density and assisting natural convection. Moreover, it is noticed that major part of literature is based on numerical investigation of shell-and-tube heat exchanger with extended surfaces, lacking the experimental investigations of proposed shell-and-tube heat exchangers. Likewise, the literature also lacks the experimental investigation of multiple passes of tube with extended surfaces in shell-and-tube heat exchanger.

This article is focused on experimental investigation of a novel shell-and-tube heat exchanger with longitudinal fins based LHS unit, which is coupled with flat plate solar collector. The computational model of novel geometrical configuration of LHS unit is previously designed and simulated by authors in [37]. The optimum design of shell-and-tube heat exchanger configuration was developed by conducting numerical analysis to examine the impact of number of tube passes, their placement in the shell, geometry of longitudinal fins and construction material on phase transition rate and thermal storage capacity of LHS unit. In this paper, the unique geometrical configuration based LHS unit is connected to flat plate solar collector with solar simulators to perform charging cycles at various operating conditions. Moreover, this paper is focused on discussing the influence of natural convection, inlet temperature and volume flow rate of HTF on temperature distribution, phase transition rate and mean power. Furthermore, this article will give an understanding into how to utilise this novel LHS unit in wide ranging domestic and commercial applications to meet large scale thermal energy demands.

2. Experimental setup and procedure

2.1 Description of experimental setup

For present study, an experimental setup is designed as illustrated in **Fig. 1**. The system is comprised of flat plate solar collector with solar simulator, latent heat storage tank, circulation centrifugal pump, a flow meter, connection to building water tank and data acquisition unit with computer.

Flat plate solar collector consists of glazing cover, stainless steel absorber, serpentine copper tubing circulation system and insulations. Transparent glass sheet with 2 mm thickness is utilised as glazing cover to dampen convection and radiation losses from solar collector. The emissivity and transmittance of glazing cover are 0.92 and 0.9, respectively. Likewise, absorber is composed of 1mm thick stainless steel S280 sheet. In order to attain high absorptivity, the absorber is coated to dark black surface. The absorptivity, emissivity and thermal conductivity of absorber are 0.9, 0.9 and 50 W/m.K, respectively. Similarly, circulation system is comprised of serpentine copper tubing, where HTF gains thermal energy from absorber. The total length, outer diameter and

thickness of copper tubing are 57.5 m, 10 mm and 1 mm, respectively. Moreover, Celotex is used as an insulating material to reduce thermal losses from sides and rear of solar collector. The thickness and thermal conductivity of insulating material are 100 mm and 0.022 W/m K, respectively.

Solar simulator is utilised to provide steady thermal energy through radiations to collector. It consists of two lightening machines with twelve quartz-halogen lamps. Each lamp can emit 1 kW radiant heat output. Kipp & Zonen CMP3 pyranometer is operated to measure average irradiance and to identify optimum distance of solar simulator from collector. Consequently, solar simulator at a distance of 2 m from collector has shown almost constant radiations at each point on collector. Further details about selection of measured points and measuring average irradiance on collector surface can be found in [38, 39]. Solar simulator has inbuilt control system to adjust radiant heat output and operation time. During experiments, solar simulator is manually operated to generate required radiant heat output in order to sustain constant outlet temperature of HTF from collector.

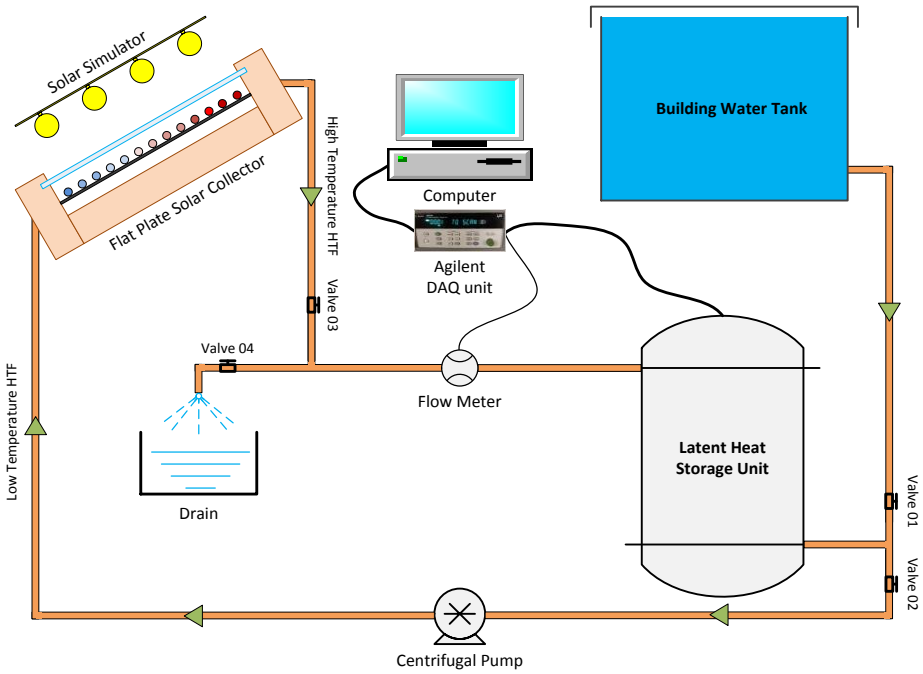

Fig. 1 Schematic representation of experimental setup

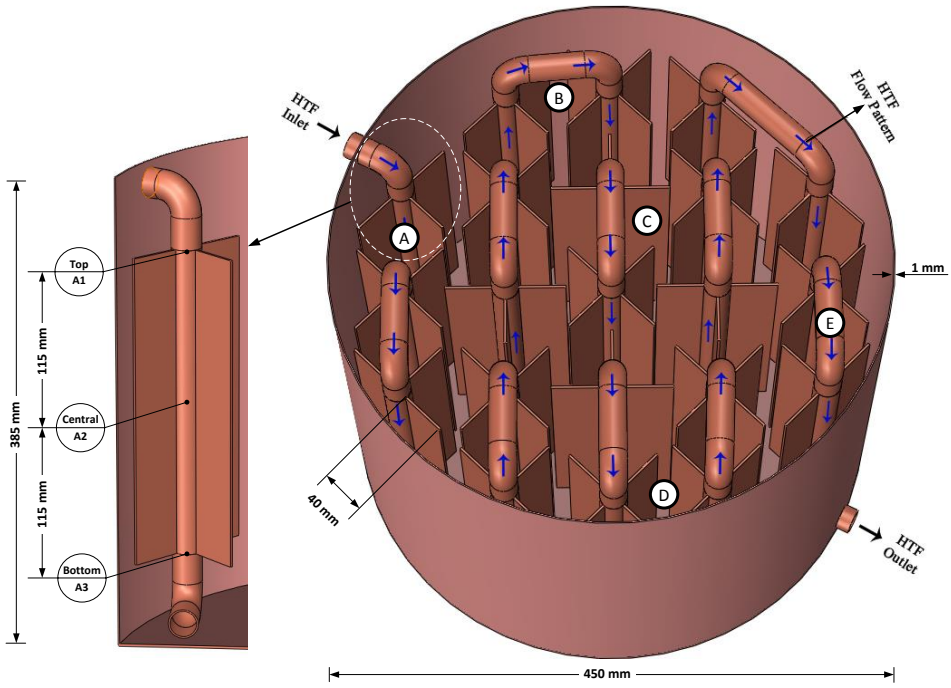

Fig. 2 Physical model of LHS unit and illustration of the vertical positioning of thermocouples at different zones A, B, C, D and E.

High temperature HTF from solar collector is directed to pass through LHS unit, where it transfers thermal energy to PCM. LHS unit consists of shell-and-tube heat exchanger with longitudinal fins and PCM, as illustrated in **Fig. 2**. Shell is made of copper and the outer diameter, height and thickness of shell are 450 mm, 385 mm and 1 mm, respectively. The exterior surface of shell is properly insulated with 50 mm thick chlorofluorocarbon-free envirofoam to reduce thermal losses to atmosphere. The tubes are made of copper and the outer diameter and thickness are 22 mm and 1 mm, respectively. The tubes have 21 passes in the shell and are connected to copper longitudinal fins of height, length and thickness as 230 mm, 40 mm and 1.5 mm, respectively. Further details about design specifications of LHS unit are provided in **Table 1**. Moreover, the detail description about geometrical orientation of tubes with longitudinal fins in shell can be found in [37]. Commercial grade paraffin (RT44HC) is filled in shell and water is employed as heat transfer fluid that is directed to run through tubes. Paraffin (RT44HC) is selected due to its high thermal storage capacity, good compatibility with copper and excellent thermo-physical stability [16, 40]. Thermo-physical properties of paraffin (RT44HC) are presented in **Table 2**.

Table 1

Specifications of shell-and-tube heat exchanger based LHS unit

Total volume of shell	V_S	60.7E+06	mm^3
Running length of tube		8.2	m
Volume occupied by tube	V_T	2.57E+06	mm^3
Surface area of longitudinal fins		3.96E+05	mm^2
Volume occupied by fins	V_F	0.29E+06	mm^3
Volume of LHS unit	$V_{LHS} = V_S - V_T - V_F$	57.8E+06	mm^3
Mass of paraffin		40	kg
Packing factor of PCM	$\frac{V_{PCM}}{V_S}$	0.824	solid
		0.942	liquid

Table 2

Thermo-physical characteristics of paraffin (RT44HC) [16, 40]		
Phase change temperature	41-44	^{o}C
Latent heat	255	(kJ/kg)
Specific heat capacity	2.0	(kJ/kg. K)
Thermal conductivity	0.2	(W/m. K) solid
	0.2	(W/m. K) liquid
Density	800	(kg/m^3) solid
	700	(kg/m^3) liquid
Coefficient of thermal expansion	0.00259	(1/K)

During charging cycle, high temperature water from solar collector is directed through tubes and heat is transferred to PCM in shell. The temperature distribution within PCM in shell is recorded by using fifteen K-type thermocouples. Five zones are selected within shell to investigate the temperature response of PCM, which are A, B, C, D and E, as shown in **Fig. 2**. The selected zones are regions closer to inlet (zone A), outlet (zone E), centre (zone C) and shell boundary (zone B and D) within LHS unit. Three thermocouples are installed at top, central and bottom position at each of five zones. The vertical distance between each thermocouple at each location is 115 mm, as shown in **Fig. 2**. Likewise, two thermocouples are mounted on copper tube at inlet and outlet of LHS unit to record the temperature response of HTF. Moreover, a turbine flow meter (Titan FT2 Hall Effect) is employed to record the volume flow rate of HTF. The accuracy of thermocouples and flow meter are ±0.18% and 1.5%, respectively. Also, a centrifugal pump (Grundfos type UPS 15-60) is utilised to circulate HTF between solar collector and LHS unit. Four flow control valves are installed before and after solar collector and LHS unit to control flow rate and direction of HTF. In order to record temperature and volume flow rate reading, a data acquisition unit (Agilent 34972A) is used to transfer data into computer. Agilent software is used to record data and display results on computer after each time step of 10 s.

2.2 Experimental procedure

During charging cycle, flow control valve 1 is switched on to direct water from mains to fill up the entire loop. The circulation of low temperature water from mains reduces the initial temperature of LHS unit to about 10 ^{o}C and therefore, a baseline for all experimental tests is established. Likewise, air release valve (not shown in **Fig. 1**) is switched on to ensure the release of trapped air in the loop. Flow control valve 4 is turned off and subsequently valve 1 is turned off to make a close loop for charging cycle. Likewise, flow control valve 2 and 3 are adjusted to operate charging cycle at specific volume flow rate. In this experimental study, four different volume flow rates of HTF are tested, which are 1.5, 2, 2.5 and 3.0 l/min. The range of volume flow rate of HTF is selected with accordance to thermal efficiency of flat plate solar collector. Further increase to volume flow rates would not generate the desired constant inlet temperature of HTF to LHS unit. Moreover, the thermal behaviour of LHS unit at various constant inlet temperature of HTF is experimentally investigated. The selected inlet temperatures values are 52, 57, 62 and 67 ^{o}C. This range is selected by considering temperature gradient of 10, 15, 20 and 25 ^{o}C between inlet temperature of HTF and melting point of PCM. The series of experimental tests conducted in this article is summarised in **Table 3**.

Solar simulator is operated to produce radiant heat output to increase thermal energy of HTF in collector. The high temperature HTF is guided to pass through the tubes in LHS unit, where heat

transfer occurs between HTF and PCM. Due to release of thermal energy to PCM, the temperature of HTF drops. Therefore, the low temperature HTF is pumped back from the outlet of LHS unit to collector to repeat the cycle. The charging cycle is completed when all thermocouples record temperature reading higher than phase change temperature.

However, it is observed that due to slow heating up process of solar collector, the temperature of HTF is gradually increased from ambient to selected range of temperature. Therefore at the start of charging cycle, entire set of 12 lamps of solar simulator are switched on to target more radiant heat at solar collector, in order to rapidly increase the temperature of HTF to selected range. Once the selected range of temperature of HTF is achieved, the solar simulator is manually operated to ensure constant inlet temperature of HTF to LHS unit.

Table 3

Range of experimental tests conducted

Set of experiments	Inlet temperature of HTF	Flow rate of HTF	Reynolds number
1-4	52, 57, 62, 67 ^{o}C	1.5 l/min	2950, 3200, 3450, 3700
5-8	52, 57, 62, 67 ^{o}C	2.0 l/min	4000, 4300, 4600, 4900
9-12	52, 57, 62, 67 ^{o}C	2.5 l/min	4950, 5350, 5750, 6150
13-16	52, 57, 62, 67 ^{o}C	3.0 l/min	5900, 6400, 6900, 7400

3. Results and discussion

3.1 Reliability and repeatability

Repeatability study is required to examine the consistency of experimental results. Therefore, a series of three charging cycle experiments are performed at constant inlet temperature of 62 ^{o}C and volume flow rate of 1.5 l/min. Transient temperature profiles are plotted for thermocouples installed at top, central and bottom positions at zone C, as shown in **Fig. 3**. It can be observed that phase transition time at all three positions for all experiments are clearly identical. Thus, it assures the reliability and repeatability of experimental results showing thermal performance. Moreover, statistical standard deviations for phase transition time at all three positions are calculated. The values of standard deviations for phase transition time at top, central and bottom positions are computed to be 0.008, 0.029 and 0.033, respectively. However, due to an expected slight variation in inlet temperature of HTF received from solar collector, the sensible heating of PCM at liquid phase shows a small variation in temperature.

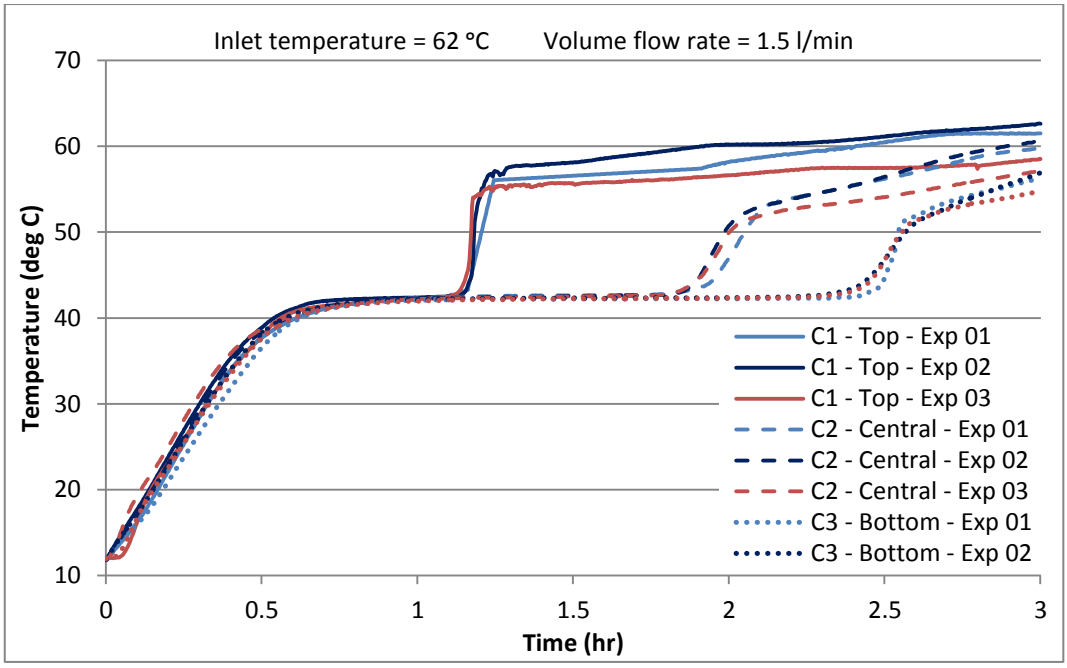

Fig. 3 Illustration of repeatability of transient temperature profiles at all three positions at zone C while charging system at constant inlet temperature of 62 ^{o}C and volume flow rate of 1.5 l/min.

3.2 Zonal temperature distribution

In order to examine the transient temperature distribution of PCM in LHS unit, temperature readings are recorded from all fifteen k-type thermocouples that are installed within LHS unit at three vertical positions at each of five zones (see **Fig. 2**). The transient temperature distribution can help in understanding the heat transfer rate and phase transition rate at different zones and positions within LHS unit. To conduct charging cycle, the high temperature HTF at 62 ^{o}C with volume flow rate of 1.5 l/min is directed from solar collector to pass through tubes in LHS unit. The initial temperature of PCM in LHS unit is nearly 10 ^{o}C.

Fig. 4 shows the pictorial depiction of phase transition performance of PCM in LHS unit. It can be noticed that due to higher temperature difference between inlet temperature of HTF and PCM, the phase transition rate at zone A is significantly higher as compared to other zones. After 0.5 hr of heat transfer, it can be noticed that top position of zone A is already either in mushy phase or liquid phase, whereas the rest of the zones are still in solid phase. Likewise, it can be observed that after 1 hr of charging cycle, the top positon of zone A is in complete liquid phase, zone B and C are in mushy phase and zone D and E are still in solid phase. Also, it can be noticed that at zone A, the PCM adjacent to tubes and longitudinal fins melts quickly and due to buoyant effect and volumetric expansion, the melted PCM rises upward to the top. Thus, it leads to rapid melting at top position whereas, central and bottom positions are still in mushy zone. After 1.5 hr, it can be seen that the top position of all zones are in liquid phase besides zone E, which is still in mushy phase. This is due to the fact that thermal energy is extracted from HTF at earlier zones and by the time HTF reaches zone E; the available thermal energy is lesser to generate higher temperature gradient. The effect of natural convection is evident in all zones. Liquid PCM at central and bottom positions rise above to top position due to density gradient and temperature difference. Thus it is expected that PCM temperature at top position will always be higher as compared to central and bottom positions. After 2.5 hr, it can be seen that the top and central positions of all zones are in liquid phase. Similarly, the bottom position at zone C is evidently showing liquid

phase, however the PCM alongside shell boundary is still in either mushy or solid phase. This is due to buoyant effect and weaker heat transfer at bottom position of LHS unit. Likewise, even after 3 hrs of charging cycle, there are still some portions of PCM in mushy phase alongside shell boundary, whereas the rest of the PCM is completely melted.

Transient temperature distribution at various positions and zones in LHS unit is represented in **Fig. 5**. It is evident from temperature profiles that due to small specific heat capacity of PCM in solid phase, the linear rise in temperature from initial value to about 40 ^{o}C is influenced by conduction heat transfer. This sensible portion of thermal energy storage is rapidly achieved. Subsequently, due to higher latent heat capacity, a comparatively slow and gradual rise in PCM temperature from 41 ^{o}C to 44 ^{o}C is observed. During this stage, as temperature increases, the phase transition of PCM from solid to mushy to liquid phase takes place. As latent portion of thermal energy is stored, an instant rise in PCM temperature is noticed, which indicates the sensible portion of thermal energy storage in liquid PCM.

It is evident from **Fig. 5** that in all zones, the increase in temperature at top position is faster as compared to central and bottom position. This is due to the fact that conduction is the dominant mode of heat transfer at earlier stages of charging cycle and consequently, phase transition from solid to liquid begins. However, with an increase in liquid fraction, natural convection becomes the dominant mode of heat transfer. Also, due to density gradient, volumetric expansion and upward rise of high temperature molecules, the temperature of PCM at top position is comparatively higher and thus phase transition rate at top is higher as compared to central and bottom positions. Likewise, as shown in **Fig. 5 (A)**, the phase transition rate at top position at zone A is 38.49% and 47.38% higher as compared zone D and zone E, respectively. This is due to the fact that temperature gradient between HTF and PCM at zone A is relatively higher and thus heat transfer is intense at zone A. Consequently, HTF transfers thermal energy to PCM at zone A and hence, the temperature gradient at zone D and zone E is comparatively smaller. Similarly, the phase transition rate at central position at zone A is reasonably higher as compared to other zones, as shown in **Fig. 5 (B)**. Besides zone A, the phase transition rates at central positions at zone B, D and E are fairly comparable. Likewise, due to natural convection and upward rise of higher temperature molecules, heat transfer is significantly smaller at bottom positions of LHS unit, especially in locations nearer to shell boundary, as shown in **Fig. 5 (C)**. It can be observed that the bottom positions at Zone B and Zone D exhibit considerably weaker phase transition rate and thus charging cycle completes after 3.12 hours.

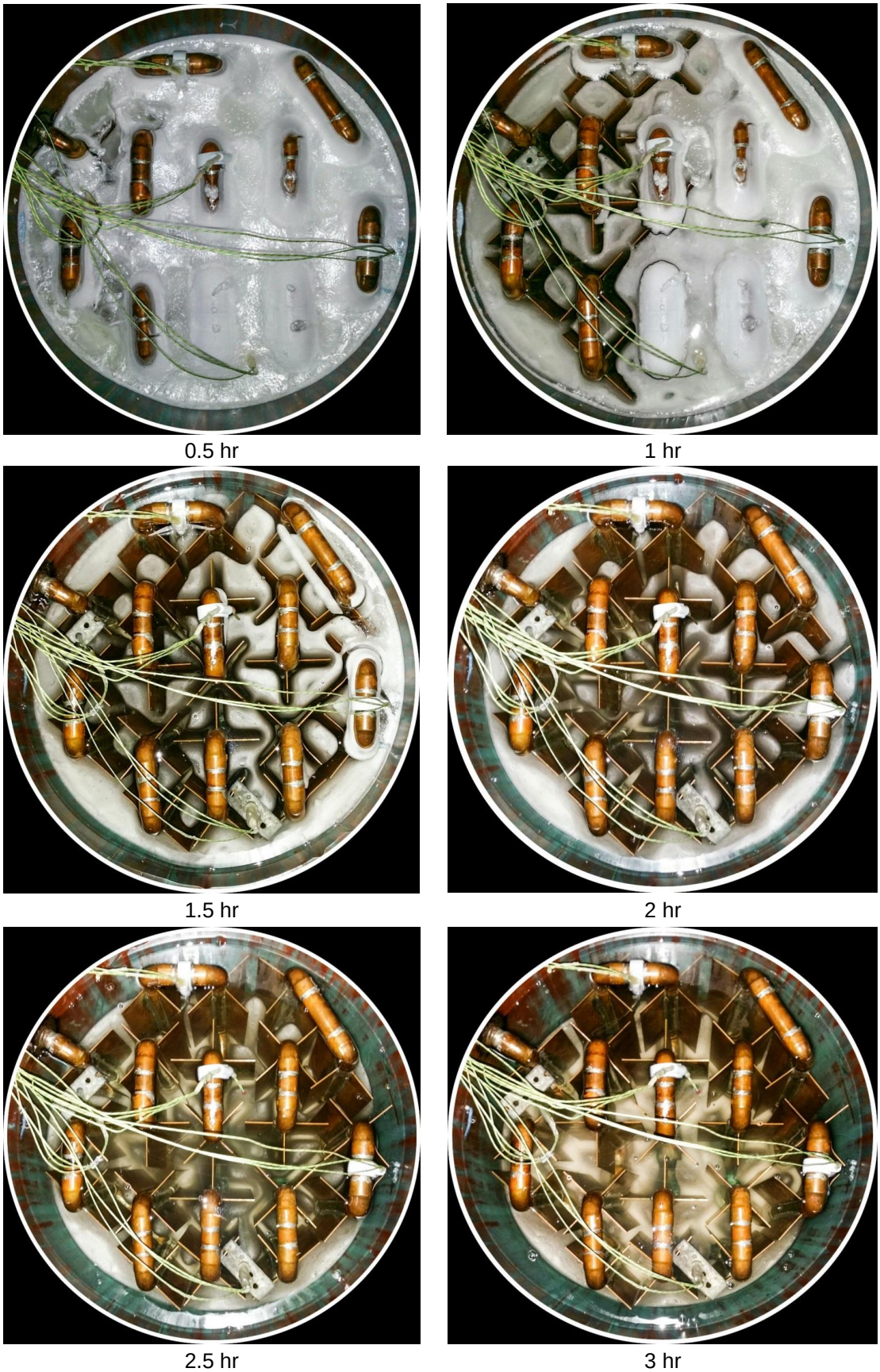

Fig. 4 Pictorial representation of PCM melting behaviour in LHS unit during charging cycle. Inlet temperature and volume flow rate of HTF are kept constant at 62 ^{o}C and 1.5 l/min, respectively.

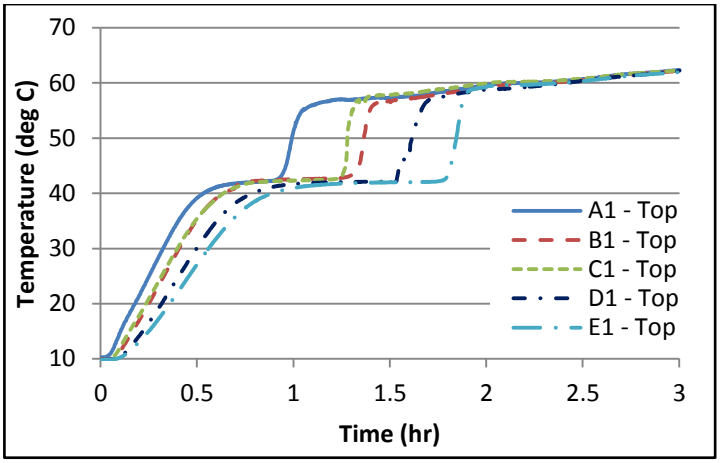

(A)

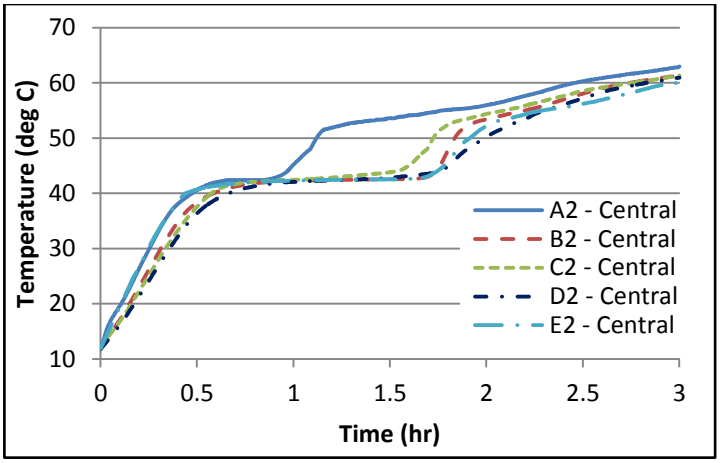

(B)

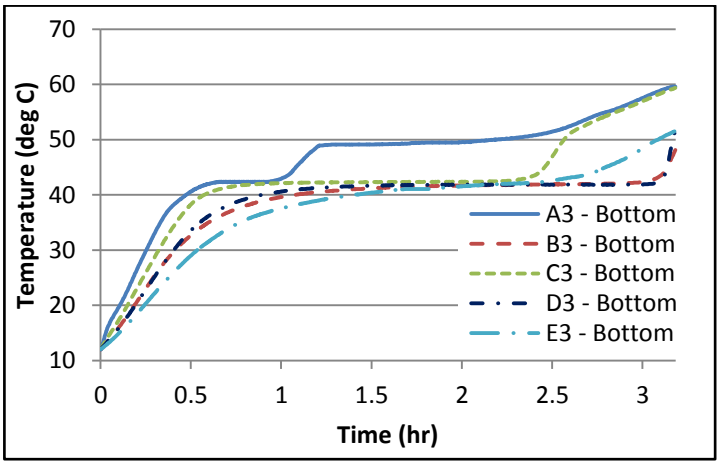

(C)

Fig. 5 Illustration of temperature profiles attained during charging cycle at all five zones (A, B, C, D and E) and all three vertical positions at each zone (1-Top, 2-Central and 3-Bottom). Inlet temperature and volume flow rate of HTF are set to 62 ^{o}C and 1.5 l/min, respectively. (A) Temperature profiles at top position at each zone, (B) central position at each zone and (C) bottom position at each zone.

3.3 Effect of inlet temperature on charging time

In order to examine the impact of weather fluctuations and solar off-peak hours on thermal performance of LHS unit, experimental tests are performed at four inlet temperatures of HTF and at constant volume flow rate of 1.5 l/min. The selected inlet temperatures of HTF are 52 ^{o}C, 57 ^{o}C, 62 ^{o}C and 67 ^{o}C. Likewise, the initial temperature of PCM is about 10 ^{o}C.

Transient temperature profiles of PCM at all three positions at zone D are illustrated in **Fig. 6**. It is evident that an increase in inlet temperature of HTF has a significant effect on phase transition rate and average temperature of PCM. Temperature gradient between PCM and HTF is the key driving force for heat transfer. With an increase in inlet temperature of HTF, higher temperature gradient can be achieved and consequently, higher heat transfer rate can be established. The accelerated heat transfer rate assures rapid phase transition from solid to liquid phase. Therefore, fraction of liquid PCM can be promptly increased, which can lead to quick natural convection and in consequence, less time will be required to complete charging cycle.

It is evident from **Fig. 6 (A)** that phase transition rate of PCM is considerably low for inlet temperature of 52 ^{o}C as compared to other inlet temperatures of HTF. Moreover, the total time required for PCM at top position at zone D to melt is 3 hr. However, with an increase in inlet temperature from 52 ^{o}C to 57 ^{o}C, 62 ^{o}C and 67 ^{o}C, the total melting time is reduced by 38.54%, 47.24% and 53.7%, respectively. Furthermore, with an increase in inlet temperature, the augmentation in sensible heating after phase transition can result in an increase in overall enthalpy of LHS unit.

As discussed in **section 3.2**, the heat transfer rate at central and bottom positions are affected due to upward rise of higher temperature molecules and buoyant effect. However, with an increase in inlet temperature, the phase transition rate can be significantly enhanced. The total time required for complete phase transition of PCM at central and bottom positions at zone D, for inlet temperature of 52 ^{o}C, are 3.14 hr and 4.48 hr, respectively (see **Fig. 6(B)** and **Fig. 6(C)**). However, with an increase in inlet temperatures to 57 ^{o}C, 62 ^{o}C and 67 ^{o}C, the total melting time at central position is reduced by 14.72%, 41.39% and 51.23%, respectively. Similarly, at bottom position, the total melting time is reduced by 15.22%, 28.49% and 45.32%, respectively. The overall reduction in melting time at zone D is calculated by taking an average of reduction in melting time at top, central and bottom positions, as shown in **Fig. 7**.

Therefore, it can be observed that the influence of an increase in inlet temperature on phase transition rate of PCM is higher at top position as compared to central and bottom positions. Additionally, it is noticed that a considerable amount of thermal energy is extracted from HTF at earlier zones, such as zone A, B and C, and thus only small fraction of thermal energy is available to generate good temperature gradient at later zones, such as zone D and E. Hence, an increase in inlet temperature can guarantee higher temperature gradient at earlier zones as well as a moderate temperature gradient at later zones.

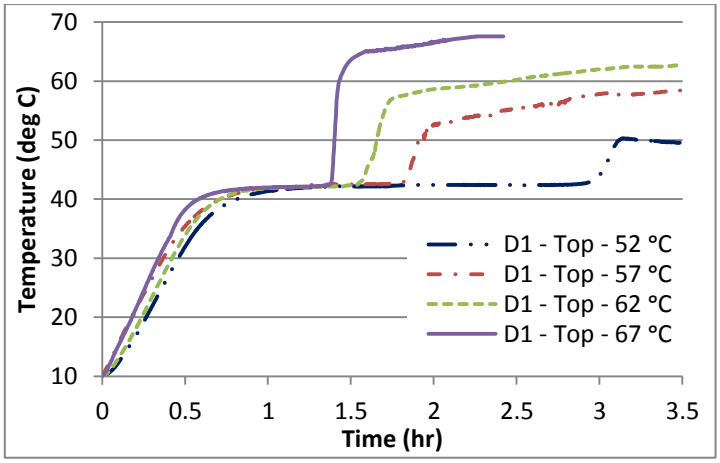

(A)

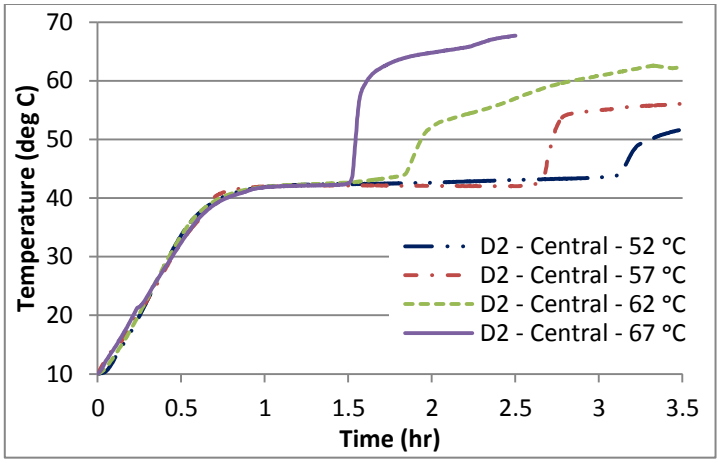

(B)

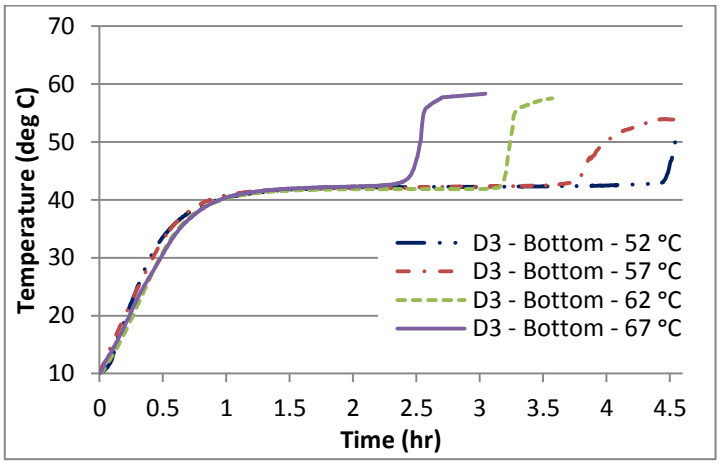

(C)

Fig. 6 Transient temperature profiles obtained from thermocouples at all three positions at zone D during charging cycle at various inlet temperatures of HTF and constant volume flow rate of 1.5 l/min.

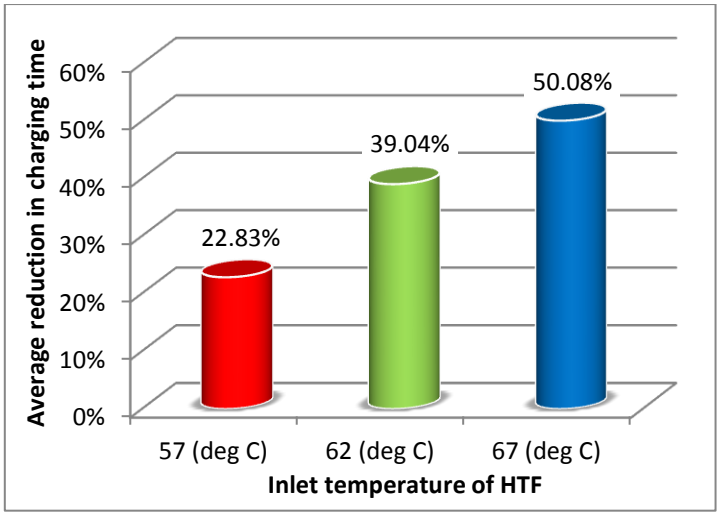

Fig. 7 Average reduction in charging time of LHS unit by increasing inlet temperature from 52 ^{o}C to 57, 62 and 67 ^{o}C.

3.4 Effect of volume flow rate on charging time

To investigate the influence of volume flow rate of HTF on phase transition rate and overall enthalpy of LHS unit, a series of sixteen experiments are conducted at four volume flow rates: 1.5, 2.0, 2.5 and 3.0 l/min and at four constant inlet temperatures: 52, 57, 62 and 67 ^{o}C, as shown in **Fig. 8**. The transient temperature profiles are obtained from thermocouples at bottom position at zone C and at central position at zone D.

As shown in **Fig. 8 (A)**, at constant inlet temperature of 52 ^{o}C, an increase in volume flow rate has no impression on enhancing the heat transfer rate at initial stages of charging cycle, which is dominated by conduction heat transfer. The reason behind is the low thermal conductivity of PCM at solid phase, due to which high thermal resistance is offered to conduction heat transfer and thus the overall heat transfer rate is affected. It is evident that the sensible heating from 15 ^{o}C to 41 ^{o}C is almost at same rate for all volume flow rates. However, the latent portion of thermal heating from 41 ^{o}C to 44 ^{o}C is highly influenced by an increase in volume flow rate. It is due to the fact that as phase transition occurs and the fraction of liquid PCM increases, natural convection starts dominating the heat transfer and therefore the overall thermal resistance offered by PCM is reduced. Thus, by increasing volume flow rate, the forced convection coefficient in tubes is improved, which enhances the heat transfer rate and reduces total time to complete charging cycle. Likewise, after the completion of latent heating, the sensible heating of liquid PCM shows an insignificant increase in temperature with an increase in volume flow rate.

Moreover, it can be observed from **Fig. 8 (A)** that by increasing volume flow rate from 1.5 l/min to 2.0, 2.5 and 3.0 l/min, the total phase transition time is reduced by 6.56%, 18.53% and 19.91%, respectively. Likewise, as shown in **Fig. 8 (B)**, the phase transition time at central position at zone D is lessened by 6.59%, 10.19% and 13.11%, respectively. Similarly, at constant inlet temperature of 57 ^{o}C, the total time required to complete phase transition at bottom position at zone C is reduced by 8.37%, 15.97% and 22.97%, respectively (see **Fig. 8 (C)**). Furthermore, the melting time at central position at zone D is decreased by 19.24%, 21.65% and 30.98%, respectively (see **Fig. 8 (D)**).

However, with higher constant inlet temperatures of 62 ^{o}C and 67 ^{o}C, the influence of volume flow rate is insignificant on phase transition rate. It is due to the fact that with higher constant inlet temperatures, a strong temperature gradient across the unit is generated, which diminishes the further enhancement due to increase in volume flow rate. As illustrated in **Fig. 8 (G)**, at constant inlet temperature of 67 ^{o}C, the melting time at bottom position at zone C is slightly reduced by 1.67%, 2.04% and 7.72% by increasing volume flow rate from 1.5 l/min to 2.0, 2.5 and 3.0 l/min, respectively. Likewise, a trivial reduction in melting time is noted at central position at zone D. Therefore, it can be deduced that at higher constant inlet temperature, the occupancy period for HTF in tubes is reduced by increasing volume flow rate and hence, the heat transfer surface remains at almost isothermal condition.

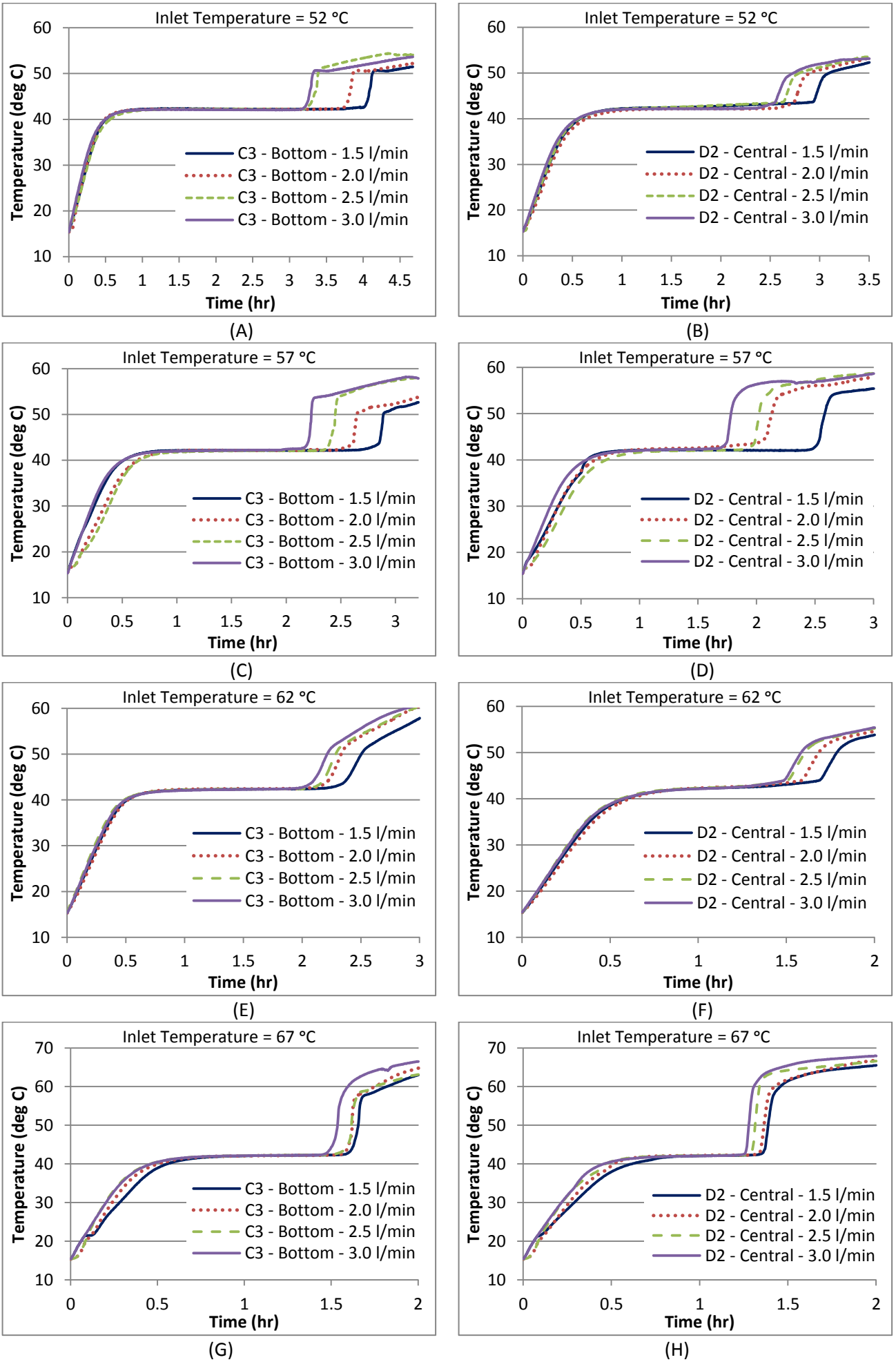

Fig. 8 Transient temperature profiles of PCM at bottom position at zone C and at central position at zone D during charging cycle at various volume flow rates and various constant inlet temperatures of HTF.

3.5 Mean power

To evaluate thermal performance of LHS unit, mean power is calculated from change in enthalpy of HTF. Thermocouples are installed at inlet and outlet of LHS unit, which can record the transient data of enthalpy change. Therefore, to calculate the total amount of thermal energy stored by LHS unit, the following subsection integral method is implemented which incorporates the variation in specific heat capacity and density of HTF with varying temperature:

$$Q_s = \sum \dot{V} \left(\frac{\rho_{in} + \rho_{out}}{2} \right) \left(\frac{C_{p,in} + C_{p,out}}{2} \right) \left(T_{HTF,in} - T_{HTF,out} \right) \Delta t \tag{1}$$

where Q_s represents the amount of thermal energy storage (kJ), $\dot{V}$ is the volume flow rate of HTF (m^3/sec), ρ is the density of HTF (kg/m^3), C_p is the specific heat capacity of HTF (kJ/kg.K), T_{HTF} shows the temperature of HTF (^oC) and Δt represents the time interval (sec) at which transient data is recorded. Further, the mean power for charging cycle is calculated as follow:

$$P_c = \frac{Q_s}{t_c} \tag{2}$$

where P_c shows the mean power (kW) and t_c is the total time elapsed (sec) during charging cycle until all thermocouples display temperature higher than phase change temperature.

For all cases, the initial temperature and mass of PCM in LHS unit is fixed. Therefore, under different thermal conditions, the mean power is highly influenced by charging time. As illustrated in **Fig. 9**, inlet temperature of HTF has an evident impact on mean power. Refer to **section 3.3**, with an increase in inlet temperature of HTF, a stronger temperature gradient is generated between HTF and PCM, which increases the heat transfer and reduces the charging time. As a result, higher mean power is generated with an increase in inlet temperature of HTF. Likewise, the increase in volume flow rate enhances the heat transfer rate and thus the charging time is reduced. As a result, a moderate increase in mean power is noticed by increasing volume flow rate of HTF.

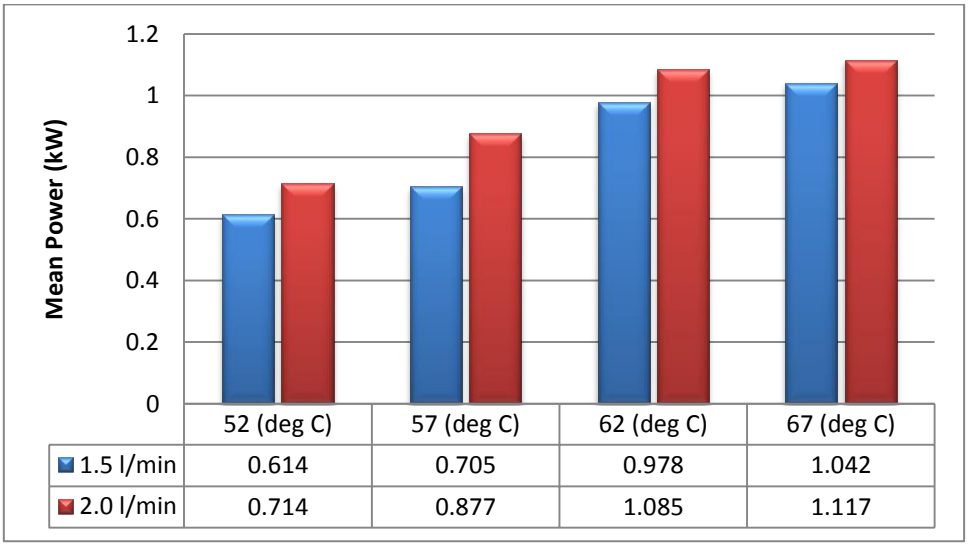

Fig. 9 Illustrating the influence of inlet temperature of HTF on mean power at two mass flow rates: 1.5 l/min and 2.0 l/min.

4. Conclusions

In this paper, experimental investigations of LHS unit connected to solar collector are performed to identify thermal performance during charging cycles. LHS unit is comprised of shell-and-tube with longitudinal fins heat exchanger and paraffin (RT44HC) as thermal storage material. Thermal performance of LHS unit is examined by conducting charging cycles at various inlet temperatures and volume flow rates of HTF. Based on experimental results, the following conclusions are derived:

- It is observed that the effective surfaces area for heat transfer and overall thermal conductivity is increased by introducing longitudinal fins in LHS unit. This novel configuration of LHS unit ensures higher thermal storage capacity and higher phase transition rate. For example, it can store 14.36 MJ of thermal energy in 3.12 hours when charged at inlet temperature of 62 ^{o}C and volume flow rate of 1.5 l/min.
- It is noticed that due to vertical orientation of shell-and-tube heat exchanger in LHS unit, the PCM at top position melts quickly as compared to central and bottom position. The reason behind is the natural convection and upward rise of high temperature liquid PCM molecules. Initially, the heat transfer is dominated by conduction. However, as the liquid fraction increases, natural convection is dominant mode of heat transfer. Moreover, longitudinal fins are employed for the reason that it does not restrict natural convection.
- Besides enthalpy gradient at top and bottom positions, it is noticed that significant quantity of thermal energy is extracted from HTF at earlier zones in LHS unit; therefore the later zones have smaller temperature gradient, which results in weaker phase transition rate. To overcome it, an increase in inlet temperature can assure better temperature gradient across entire LHS unit and therefore, phase transition rate can be significantly increased. For example, the average melting time is reduced by 22.83%, 39.04% and 50.08% as the inlet temperature is increased from 52 ^{o}C to 57, 62 and 67 ^{o}C, respectively. Likewise, the mean power is increased by 59.28% and 69.71% as the inlet temperature is increased from 52 ^{o}C to 62 ^{o}C and 67 ^{o}C, respectively.
- An increase in volume flow rate has a relatively moderate influence on thermal performance. The reason behind is that as natural convection starts dominating the heat transfer in LHS unit, an increase in volume flow rate of HTF in tubes enhances the forced convection coefficient in tubes and thus heat transfer improves. For example, at constant inlet temperature of 57 ^{o}C, the heat transfer is improved by increasing volume flow rate from 1.5 l/min to 2, 2.5 and 3 l/min and consequently, the melting time is reduced by 19.24%, 21.65% and 30.98%, respectively. However, with an increase in constant inlet temperature of HTF, the influence of volume flow rate on phase transition rate weakens. For example, at constant inlet temperature of 67 ^{o}C, as the volume flow rate is increased, the melting time is slightly reduced by 1.67%, 2.04% and 7.72%, respectively.
- Due to an upsurge in phase transition rate, the higher thermal storage capacity of LHS unit is completely charged in as less as 3 hours. Therefore, this novel LHS unit can provide time, spatial and financial benefits in range of household and industrial applications. Furthermore, depending on applications, thermal storage capacity and mean power can be enlarged by assembling several LHS units in parallel sequence. In this manner, LHS unit can serve as a versatile element for larger systems such as solar power plants, waste heat recovery and domestic heating systems.

Acknowledgement

The authors would like to acknowledge Bournemouth University, UK and National University of Sciences and Technology (NUST), Pakistan for their direct funding for conducting this research and the support they have provided.

References

[1] International Energy Agency (IEA). Energy and Climate Change 21st UN Conference of the Parties (COP21). Paris2015.
[2] Suranovic S. Fossil fuel addiction and the implications for climate change policy. Global Environmental Change. 2013;23:598-608.
[3] Jacobson MZ. Review of solutions to global warming, air pollution, and energy security. Energy & Environmental Science. 2009;2:148-73.
[4] Modi A, Bühler F, Andreasen JG, Haglind F. A review of solar energy based heat and power generation systems. Renewable and Sustainable Energy Reviews. 2017;67:1047-64.
[5] Sharma A, Tyagi VV, Chen C, Buddhi D. Review on thermal energy storage with phase change materials and applications. Renewable and Sustainable energy reviews. 2009;13:318-45.
[6] da Cunha JP, Eames P. Thermal energy storage for low and medium temperature applications using phase change materials–a review. Applied Energy. 2016;177:227-38.
[7] Tian Y, Zhao C-Y. A review of solar collectors and thermal energy storage in solar thermal applications. Applied Energy. 2013;104:538-53.
[8] Shukla A, Kant K, Sharma A. Solar Still with latent heat energy storage: A review. Innovative Food Science & Emerging Technologies. 2017.
[9] Pelay U, Luo L, Fan Y, Stitou D, Rood M. Thermal energy storage systems for concentrated solar power plants. Renewable and Sustainable Energy Reviews. 2017;79:82-100.
[10] Miró L, Gasia J, Cabeza LF. Thermal energy storage (TES) for industrial waste heat (IWH) recovery: a review. Applied Energy. 2016;179:284-301.
[11] Waqas A, Din ZU. Phase change material (PCM) storage for free cooling of buildings—a review. Renewable and sustainable energy reviews. 2013;18:607-25.
[12] Rabha D, Muthukumar P. Performance studies on a forced convection solar dryer integrated with a paraffin wax–based latent heat storage system. Solar Energy. 2017;149:214-26.
[13] Park S, Woo S, Shon J, Lee K. Experimental study on heat storage system using phase-change material in a diesel engine. Energy. 2017;119:1108-18.
[14] Cabeza LF, Castell A, Barreneche Cd, De Gracia A, Fernández A. Materials used as PCM in thermal energy storage in buildings: a review. Renewable and Sustainable Energy Reviews. 2011;15:1675-95.
[15] Dhaidan NS, Khodadadi J. Melting and convection of phase change materials in different shape containers: A review. Renewable and Sustainable Energy Reviews. 2015;43:449-77.
[16] Khan Z, Khan Z, Ghafoor A. A review of performance enhancement of PCM based latent heat storage system within the context of materials, thermal stability and compatibility. Energy Conversion and Management. 2016;115:132-58.
[17] Liu L, Su D, Tang Y, Fang G. Thermal conductivity enhancement of phase change materials for thermal energy storage: A review. Renewable and Sustainable Energy Reviews. 2016;62:305-17.
[18] Liu C, Rao Z, Zhao J, Huo Y, Li Y. Review on nanoencapsulated phase change materials: Preparation, characterization and heat transfer enhancement. Nano Energy. 2015;13:814-26.
[19] Giro-Paloma J, Martínez M, Cabeza LF, Fernández AI. Types, methods, techniques, and applications for microencapsulated phase change materials (MPCM): a review. Renewable and Sustainable Energy Reviews. 2016;53:1059-75.
[20] Agyenim F, Hewitt N, Eames P, Smyth M. A review of materials, heat transfer and phase change problem formulation for latent heat thermal energy storage systems (LHTESS). Renewable and sustainable energy reviews. 2010;14:615-28.
[21] Wang W-W, Zhang K, Wang L-B, He Y-L. Numerical study of the heat charging and discharging characteristics of a shell-and-tube phase change heat storage unit. Applied Thermal Engineering. 2013;58:542-53.
[22] Tay N, Bruno F, Belusko M. Experimental validation of a CFD model for tubes in a phase change thermal energy storage system. International Journal of Heat and Mass Transfer. 2012;55:574-85.

[23] Hosseini M, Ranjbar A, Sedighi K, Rahimi M. A combined experimental and computational study on the melting behavior of a medium temperature phase change storage material inside shell and tube heat exchanger. International Communications in Heat and Mass Transfer. 2012;39:1416-24.
[24] Meng Z, Zhang P. Experimental and numerical investigation of a tube-in-tank latent thermal energy storage unit using composite PCM. Applied Energy. 2017;190:524-39.
[25] Esapour M, Hosseini M, Ranjbar A, Pahamli Y, Bahrampoury R. Phase change in multi-tube heat exchangers. Renewable Energy. 2016;85:1017-25.
[26] Luo K, Yao F-J, Yi H-L, Tan H-P. Lattice Boltzmann simulation of convection melting in complex heat storage systems filled with phase change materials. Applied Thermal Engineering. 2015;86:238-50.
[27] Rathod MK, Banerjee J. Thermal performance enhancement of shell and tube Latent Heat Storage Unit using longitudinal fins. Applied thermal engineering. 2015;75:1084-92.
[28] Yuan Y, Cao X, Xiang B, Du Y. Effect of installation angle of fins on melting characteristics of annular unit for latent heat thermal energy storage. Solar Energy. 2016;136:365-78.
[29] Li Z, Wu Z-G. Analysis of HTFs, PCMs and fins effects on the thermal performance of shell–tube thermal energy storage units. Solar Energy. 2015;122:382-95.
[30] Darzi AAR, Jourabian M, Farhadi M. Melting and solidification of PCM enhanced by radial conductive fins and nanoparticles in cylindrical annulus. Energy Conversion and Management. 2016;118:253-63.
[31] Tao Y, He Y. Effects of natural convection on latent heat storage performance of salt in a horizontal concentric tube. Applied Energy. 2015;143:38-46.
[32] Wang P, Yao H, Lan Z, Peng Z, Huang Y, Ding Y. Numerical investigation of PCM melting process in sleeve tube with internal fins. Energy Conversion and Management. 2016;110:428-35.
[33] Liu C, Groulx D. Experimental study of the phase change heat transfer inside a horizontal cylindrical latent heat energy storage system. International Journal of Thermal Sciences. 2014;82:100-10.
[34] Tay NHS, Bruno F, Belusko M. Comparison of pinned and finned tubes in a phase change thermal energy storage system using CFD. Applied Energy. 2013;104:79-86.
[35] Caron-Soupart A, Fourmigué J-F, Marty P, Couturier R. Performance analysis of thermal energy storage systems using phase change material. Applied Thermal Engineering. 2016;98:1286-96.
[36] Agyenim F, Eames P, Smyth M. A comparison of heat transfer enhancement in a medium temperature thermal energy storage heat exchanger using fins. Solar Energy. 2009;83:1509-20.
[37] Khan Z, Khan Z, Tabeshf K. Parametric investigations to enhance thermal performance of paraffin through a novel geometrical configuration of shell and tube latent thermal storage system. Energy Conversion and Management. 2016;127:355-65.
[38] Helvaci H, Khan ZA. Mathematical modelling and simulation of multiphase flow in a flat plate solar energy collector. Energy Conversion and Management. 2015;106:139-50.
[39] Helvaci H, Khan ZA. Experimental study of thermodynamic assessment of a small scale solar thermal system. Energy Conversion and Management. 2016;117:567-76.
[40] Rubitherm® Technologies GmbH, http://www.rubitherm.eu/en/. 2017.